Comparisons of thermospheric high-latitude nitric oxide observations from SNOE and global auroral X-ray bremsstrahlung observations from PIXIE

S. M. Petrinec and W. L. Imhof
Lockheed Martin Advanced Technology Center, Palo Alto, California, USA

C. A. Barth, K. D. Mankoff, and D. N. Baker
Laboratory for Atmospheric and Space Physics, Boulder, Colorado, USA

J. G. Luhmann
Space Sciences Laboratory, University of California, Berkeley, Berkeley, California, USA

Received 18 April 2002; revised 30 October 2002; accepted 6 January 2003; published 18 March 2003.

[1] Three years (March 1998 through March 2001) of nitric oxide (NO) observations in the Northern Hemispheric thermosphere (90–170 km) as made by the Student Nitric Oxide Explorer (SNOE) spacecraft are compared in a broad statistical analysis with the daily-averaged northern auroral bremsstrahlung x-ray observations, which are taken to be a good proxy for the population of precipitating energetic electrons. The latter are made by the Polar Ionospheric X-ray Imaging Experiment (PIXIE) on board the NASA GGS Polar spacecraft. A modest correlation between these two data sets is found, indicating that about 20–40% of the variation in the number density of thermospheric nitric oxide at high latitudes is caused by variations in the precipitation of energetic particles from the magnetosphere into the auroral regions of the ionosphere. Time delays between the two data sets are examined in this study, as well as the altitude profile of the nitric oxide observations. Differences in the response and recovery times in the two data sets are also carefully considered along with hemispheric asymmetries as a function of season, leading to stronger correlations which are then discussed in terms of the properties of the data sets used. *INDEX TERMS:* 2716 Magnetospheric Physics: Energetic particles, precipitating; 2736 Magnetospheric Physics: Magnetosphere/ionosphere interactions; 2437 Ionosphere: Ionospheric dynamics; 2407 Ionosphere: Auroral ionosphere (2704); 2455 Ionosphere: Particle precipitation; *KEYWORDS:* M-I coupling, thermosphere, ionosphere, nitric oxide, bremsstrahlung

Citation: Petrinec, S. M., W. L. Imhof, C. A. Barth, K. D. Mankoff, D. N. Baker, and J. G. Luhmann, Comparisons of thermospheric high-latitude nitric oxide observations from SNOE and global auroral X-ray bremsstrahlung observations from PIXIE, *J. Geophys. Res.*, *108*(A3), 1123, doi:10.1029/2002JA009451, 2003.

1. Introduction

[2] Several recent papers [*Callis*, 2001; *Baker et al.*, 2001, and references therein] have stressed the need to include particle precipitation effects in atmospheric models. On the basis of this prior work, it is important to study atmospheric chemistry changes due to external (i.e., magnetospheric, heliospheric, and solar) phenomena in order to distinguish such effects from other possible sources of short- and long-term atmospheric changes. An important aspect, then, is understanding the causes and effects of solar, galactic, and magnetospheric particle precipitation (over the entire energy spectrum) into the terrestrial atmosphere. Much attention has been paid to ozone levels in the middle atmosphere, and short-term variations have been found to coincide with large solar proton events [*Weeks et al.*, 1972; *Heath et al.*, 1977; *Reagan et al.*, 1981; *Solomon et al.*, 1983; *Jackman et al.*, 1990, 2001]. Such events produce considerable changes to the HO_x and NO_x atmospheric constituents [e.g., *Crutzen et al.*, 1975; *McPeters*, 1986; *Vitt and Jackman*, 1996; *Jackman et al.*, 2001], which causes catalytic destruction of ozone. Other types of precipitation cause changes even deeper into the atmosphere [*Lastovicka*, 1996, and references therein]. At higher altitudes the levels of minor chemical species (i.e., NO_x) have also been of keen interest, because of downward transport to the middle atmosphere, especially in the respective high-latitude regions during winter months [*Callis et al.*, 1996; *Randall et al.*, 1998, 2001]. Nitric oxide is an especially important minor species of the lower thermosphere and is created by almost any injection of energy. The long lifetime of NO allows it to be used as a tracer of atmospheric dynamics [*Barth*, 1992].

[3] Recently, case studies of energetic electron precipitation as observed from the vantage point of space during

0148-0227/03/2002JA009451$09.00

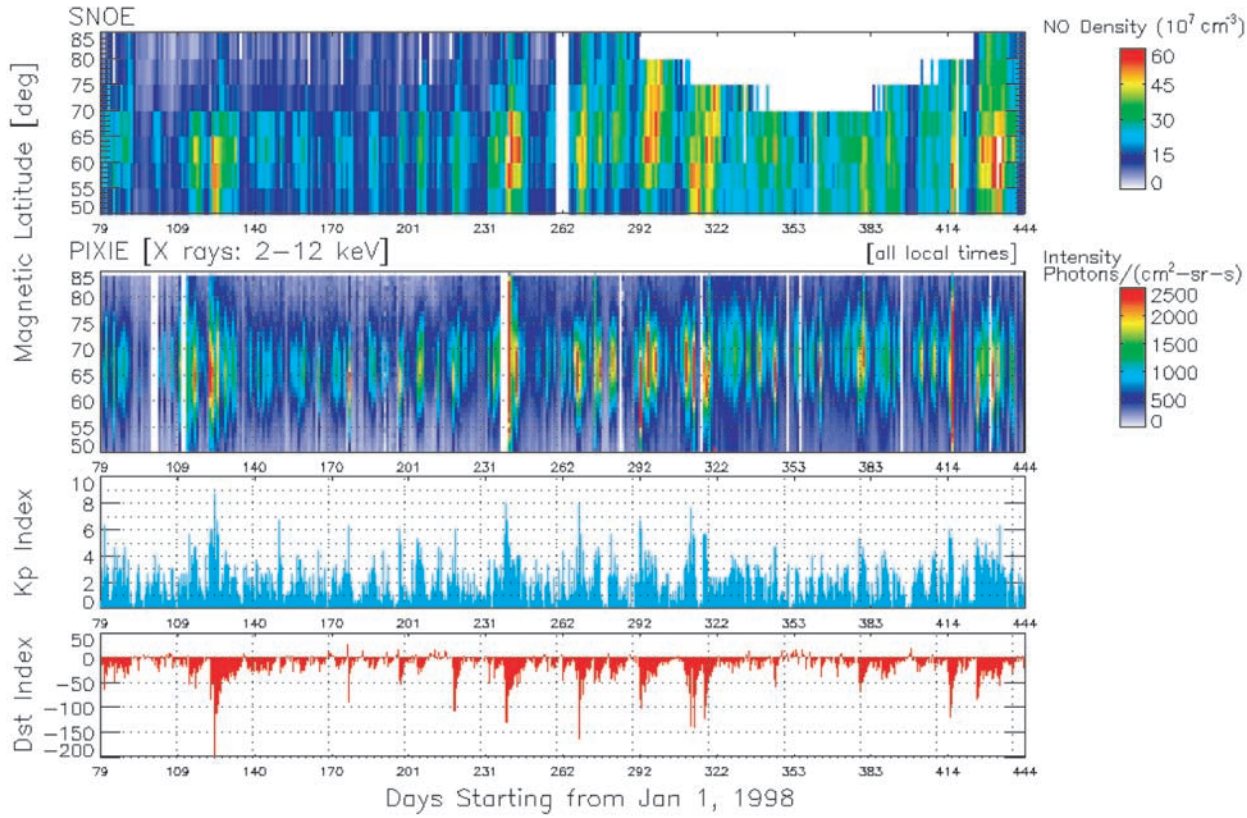

Figure 1. Keograms from the first year of SNOE operation (20 March 1998 through 19 March 1999). The top panel shows daily-averaged nitric oxide observations in the northern auroral region, at 106 km altitude. Data are from the SNOE satellite. The second panel shows daily-averaged Northern Hemisphere auroral bremsstrahlung due to energetic electron precipitation. Averages include all local times. Data are from the front chamber of the PIXIE instrument. The third panel shows the planetary geomagnetic activity level, as portrayed by the *Kp* index. The bottom panel shows ring current activity, as represented by the *Dst* index.

geomagnetic storms were carried out by *Frahm et al.* [1997] using the Particle Environment Monitor (PEM) experiment on board the Upper Atmosphere Research Satellite (UARS). These observations were compared with quiet-time observations, and a computational model (coupled electron-photon cross section (CEPXS)/one-dimensional multigroup Legendre discrete (ONELD) multistream discrete ordinates code, as described by *Lorence et al.* [1990] and *Lorence* [1992]) was used by Frahm et al. to illustrate that the combined electron precipitation and bremsstrahlung radiation during geomagnetically active times can significantly affect the ion production rate deep within the atmosphere (reaching down to 20 km altitude).

[4] In the present statistical study, three years of high-latitude (Northern Hemisphere) Student Nitric Oxide Explorer (SNOE) data are used in coordination with auroral bremsstrahlung X-ray data (as a proxy for the amount of precipitation of magnetospheric energetic electrons into the lower thermosphere, at ~110 km altitude) as observed concurrently by the Polar Ionospheric X-ray Imaging Experiment (PIXIE). The energy of the emitted bremsstrahlung radiation is less than or equal to the kinetic energy of the precipitating electrons which produced the radiation [cf. *Berger and Seltzer*, 1972]. The precipitating electrons span a large range of energies; from tens of eV up to a few MeV [cf. *Frahm et al.*, 1997]. The PIXIE instrument is the first X-ray imager to be able to image the entire auroral oval at once, providing excellent coverage for use in both statistical [*Petrinec et al.*, 1999, 2000; *Anderson et al.*, 2001] and case [*Imhof et al.*, 2000, 2001; *Anderson et al.*, 2000; *Østgaard et al.*, 1999, 2000a, 2000b] studies. We examine here how the global electron precipitation from the magnetosphere affects thermospheric chemistry (in particular, NO) as a function of altitude and a variety of temporal scales (long-term, seasonal, transport processes, and gain and loss rates).

2. Instrumentation and Data Sets

[5] The SNOE spacecraft was launched on 26 February 1998 and is in a 580 km, Sun-synchronous orbit at approximately 1030 LT and 97.75 degrees inclination. The spacecraft spins at five revolutions per minute with the spin axis normal to the orbit plane. The ultraviolet spectrometer (UVS) on board the SNOE spacecraft consists of an Ebert-Fastie spectrometer, an off-axis telescope, and two Hamamatsu phototube detectors. This instrument primarily measures the nitric oxide density between the altitudes of 90 and 170 km in the lower thermosphere by observing the

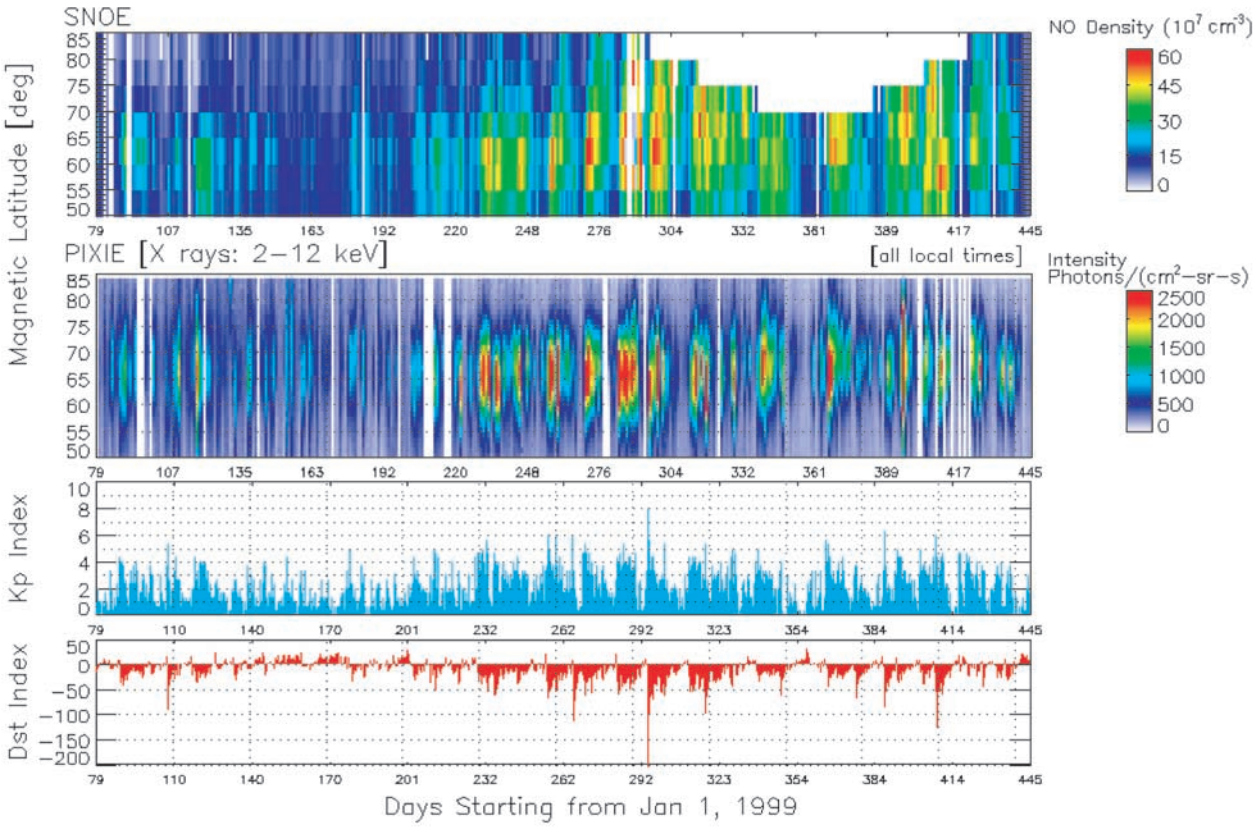

Figure 2. Same as Figure 1, but for the second year of SNOE operations (20 March 1999 through 19 March 2000).

(1,0) and (0,1) gamma bands in daylight. The UVS is mounted with its optical axis perpendicular to the spin axis of the spacecraft. The telescope images the entrance slit of the spectrometer on the limb such that the long axis of the slit lies parallel to the horizon. The image of the slit on the limb corresponds to a thermospheric altitude region of 3.5 km, which is the fundamental vertical resolution of the instrument. The grating in the spectrometer places the (1,0) gamma band (215 nm) on one detector and the (0,1) gamma band (237 nm) on the other detector. The integration time is 2.41 ms, and observations are made during only a small fraction of each satellite spin period. The UVS is similar in design to instruments flown on the Solar Mesospheric Explorer (SME), Pioneer Venus, and several rocket flights. Additional information is given by *Solomon et al.* [1996] and *Bailey et al.* [1996].

[6] PIXIE is a multiple pinhole camera on board the NASA GGS Polar spacecraft, composed of two gas proportional counters which record the position of origin and energy for each incident X ray (designed to measure 2–12 keV bremsstrahlung X rays in the front chamber; 10–60 keV bremsstrahlung X rays in the rear chamber). The camera has four stacked focal planes; two in each chamber. Each detected X ray is time-tagged along with the position and energy of the X ray, and is telemetered to Earth. This process allows the exposure time to be defined by the user. In this study, only X rays from the front chamber are analyzed. The position of each recorded X ray is traced back to its assumed point of origin in the Earth's ionosphere at 110 km altitude (the altitude at which the majority of bremsstrahlung from electron precipitation is assumed to be produced). As mentioned above, PIXIE has a very large field of view, so that nearly the entire Northern Hemisphere of the Earth can be seen at once when POLAR is near apogee ($\sim$9 R_E). Higher spatial resolution of the Southern Hemisphere is obtained at perigee ($\sim$1.8 R_E), but the viewing coverage is not always complete. The extensive coverage by PIXIE allows for greater capability in distinguishing temporal from spatial variations in the auroral observations. PIXIE is shut off when POLAR is in the radiation belts, and the front chamber is duty cycled to minimize problems with high-voltage power supply glitches. Additional information regarding the PIXIE instrument is given by *Imhof et al.* [1995].

[7] The X rays observed by PIXIE are traced back to the Earth's ionosphere (as noted above) and are assigned a geomagnetic latitude and local time. The X-ray intensity from a given region of the ionosphere is calculated from the dead-time-corrected counts observed within that given region per unit of time, per square centimeter of sampling area (which depends on the number of pinholes used), per steradian (calculated as the ionospheric area projected onto a plane oriented perpendicular to the look-direction, divided by the square of the distance of PIXIE from the region of interest), and corrected by the efficiency of the X-ray detector.

[8] The geomagnetic indices (*Kp* and *Dst*) are provided via the World Data Center Web site. These are used to

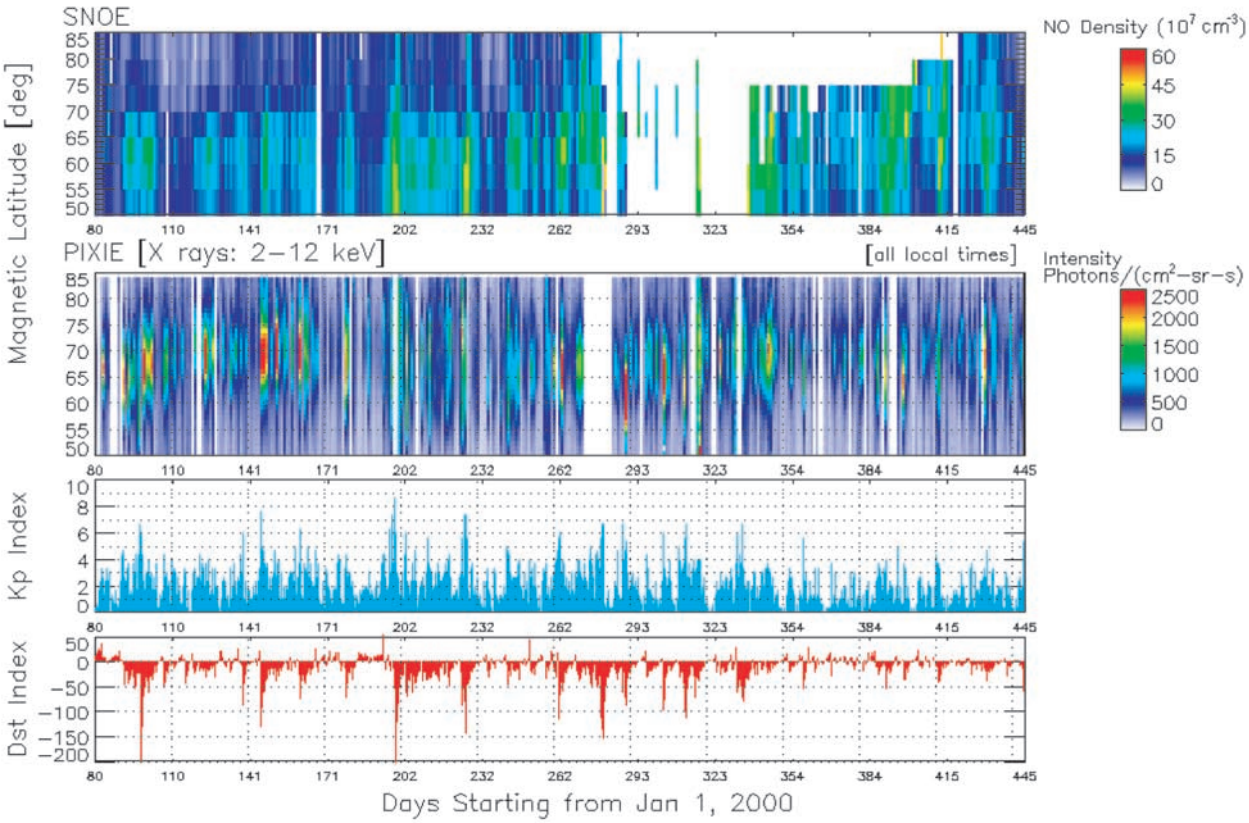

Figure 3. Same as Figure 1, but for the third year of SNOE operations (20 March 2000 through 19 March 2001).

identify storms and other major geomagnetic disturbances and are plotted for contextual reference.

3. Observations and Analysis

[9] Figure 1 shows a year of observations from the PIXIE and SNOE instruments, along with geomagnetic indices. The top panel shows daily-averaged NO densities at an altitude of 106 km (the altitude at which the NO density is highest) as a function of magnetic latitude, in the Northern Hemisphere polar region (50–85 degrees). Sixfold to sevenfold increases of the thermospheric NO density can be observed during specific geomagnetic storms. There is a period of time for which there are some latitudes not sampled by SNOE. This is because SNOE only sees the daylit portion of the ionosphere, and the latitudinal gaps correspond to positions where the ionosphere was in darkness. The second panel shows the PIXIE daily-averaged lower thermospheric X-ray emissions, also as a function of magnetic latitude. The PIXIE observations are obtained from the front chamber, for X-ray energies between 2 and 8 keV (the actual energy range varies somewhat with instrument temperature, high-voltage level, and instrument age). The PIXIE intensities shown are averaged over all local times. Gaps in the data correspond to times when either the Polar spacecraft attitude vector was rotated 180° to avoid direct sunlight on some of the instruments, or incidents when large in situ fluxes of energetic solar particles caused PIXIE to enter auto-shutoff mode. The third panel indicates planetary geomagnetic activity as represented by the 3-hour *Kp* index, while the bottom panel represents the ring current activity as represented by the *Dst* index. It can be seen that enhancements of geomagnetic activity lead to the precipitation of energetic particles into the auroral ionosphere (as determined from the bremsstrahlung emissions [*Petrinec et al.*, 1999]), as well as enhancements in the density of thermospheric nitric oxide. It can easily be seen that both strong and weak geomagnetic storms cause variations in the NO density. The format for Figure 2 is the same as that of Figure 1, but is for the second year of the SNOE mission, while Figure 3 corresponds to the third year of SNOE operation. The gap in the SNOE observations in Figure 3 pertains to a period of time when the instrument was being calibrated against celestial sources. It can also be seen in Figures 1–3 that although the timings of enhancements in the PIXIE and SNOE data sets are similar, there are differences in the latitudinal extent as well as the latitude of greatest emission (PIXIE daily-averaged X-ray intensities are plotted with a latitudinal resolution of 1°; SNOE with a resolution of 5°). Much of this difference is due to the nature of the data sets. The X rays are integrated over all local times, whereas the NO is observed only at one local time (1030). Most auroral precipitation occurs on the nightside, and the effects on the thermospheric NO are only observed with corotation to 1030 LT. Orbital coverage (PIXIE only observes the north-

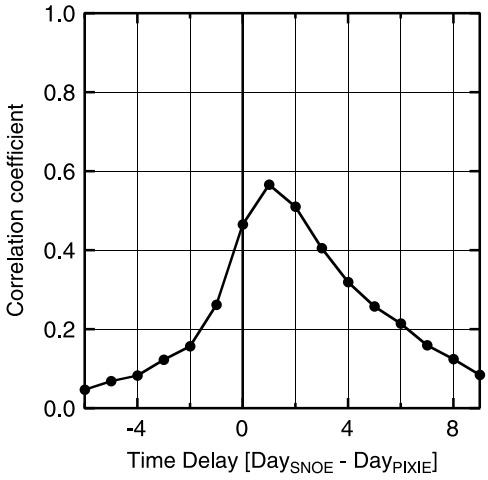

Figure 4. Variation of the correlation coefficient between the daily-averaged nitric oxide densities (at 106 km altitude) and the X-ray intensities, as a function of the delay time between the two data sets, over the 3-year time span. Positive time delays correspond to nitric oxide observations which lag the X-ray observations.

ern auroral region about 10 hours of each 18-hour orbit) also introduces the substantial probability that PIXIE has missed a significant amount of auroral precipitation, which affects the daily average (both in magnitude and latitudinal distribution).

[10] In spite of the differences in the collection of the data sets, a more quantitative assessment is made by averaging the daily NO density observations and the daily X-ray intensities over the latitude range shown in Figures 1–3, for the entire 3-year duration. The daily-averaged SNOE observations have been weighted by the latitudes covered. The correlation coefficient between the logarithm of the X-ray emissions and logarithm of the NO densities over the 3 years is 0.46.

[11] In Figure 4, correlations between the daily averages are performed with varying time delays between the two data sets. The best correlation (0.57) is found with a 1-day delay in the SNOE data set with respect to the PIXIE data set (Figure 5). This is consistent with the study of *Solomon et al.* [1999], which found that the best correlation between DMSP and SNOE observations was achieved with a 1-day delay of the SNOE data set. One reason for this time delay is that it takes several hours for the changes in NO caused by auroral precipitation (often strongest near local midnight) to rotate from the nightside to the local time which is observable by SNOE (1030 LT). In addition, the enhanced NO has a considerable lifetime; large enhancements can persist for longer than a day (especially during the winter), whereas the auroral precipitation varies on a much faster timescale. The photodissociation frequency calculated by *Minschwaner and Siskind* [1993] is 5.8×10^{-6} s^{-1}. With laboratory data from *Murray et al.* [1994], the frequency becomes 7.1×10^{-6} s^{-1}. Since each photodissociation destroys an NO molecule and produces an N atom which then destroys another NO molecule, the effective dissociation frequency is 1.4×10^{-5} s^{-1}, resulting in an effective lifetime of NO of 19.6 hours (decreasing only in daylight). Thus, for these reasons the SNOE data set delayed by 1 day is found to be most strongly correlated with the PIXIE auroral emissions.

[12] Solar proton events (SPEs) are also known to have some influence on nitric oxide production in the lower thermosphere [*Reagan et al.*, 1981]. Large events increase the rate of ion production by as much as about 10% at about 100 km, based upon the study of *Reid et al.* [1991]. A complete, quantitative assessment of the influence of SPEs on the NO densities at lower thermospheric altitudes, however, is beyond the scope of this study.

[13] The X rays are expected to arise predominantly from thermospheric altitudes between 100 and 110 km, due to the precipitation of several keV electrons, as shown by the atmospheric profiles for precipitating energetic electrons in Figure 6a. This figure is adapted from the results of *Rees* [1992] and displays profiles for unidirectional, monoenergetic precipitating electrons of flux 10^8 el/cm^2-s. Figure 6b shows the rates of polar NO production (predominantly $N(^2D) + O_2 \rightarrow NO + O$ and $N(^4S) + O_2 \rightarrow NO + O$) and loss (predominantly $NO + N(^4S) \rightarrow N_2 + O$, $NO + O_2^+ \rightarrow NO^+ + O_2$, and $NO + h\nu \rightarrow N(^4S) + O$). A comprehensive description of the processes which produce and destroy NO is provided by *Barth* [1992]. Although these rates help determine the amount of NO present in the lower thermosphere, variations in solar illumination and auroral particle precipitation are known to cause large variations in the amount of NO present [*Barth*, 1992]. Figure 6c shows model results of NO density altitude profiles which include a variety of values for the precipitating electron flux (dashed lines), along with the SNOE northern polar region NO observations over the first 3 years of the mission. The SNOE observations show a broad peak between 106 and 110 km, which is only slightly higher in altitude than the peak in the model results (which maximize at ~103 km). Interestingly, though, a comparison of X-ray emissions and

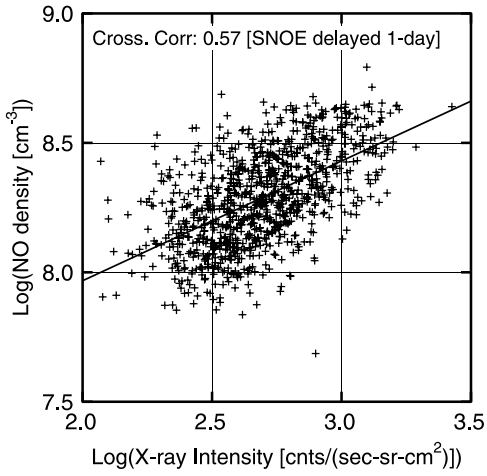

Figure 5. Daily-averaged Northern Hemispheric nitric oxide densities at 106 km altitude spanning 3 years, plotted versus the daily-averaged intensity of northern auroral bremsstrahlung. Magnetic latitudes are 50°–85°, and all local times for the bremsstrahlung are used in the analysis. A 1-day offset is included between the NO observations and the X-ray emissions (i.e., yesterday's X-ray emissions are paired with today's NO observations).

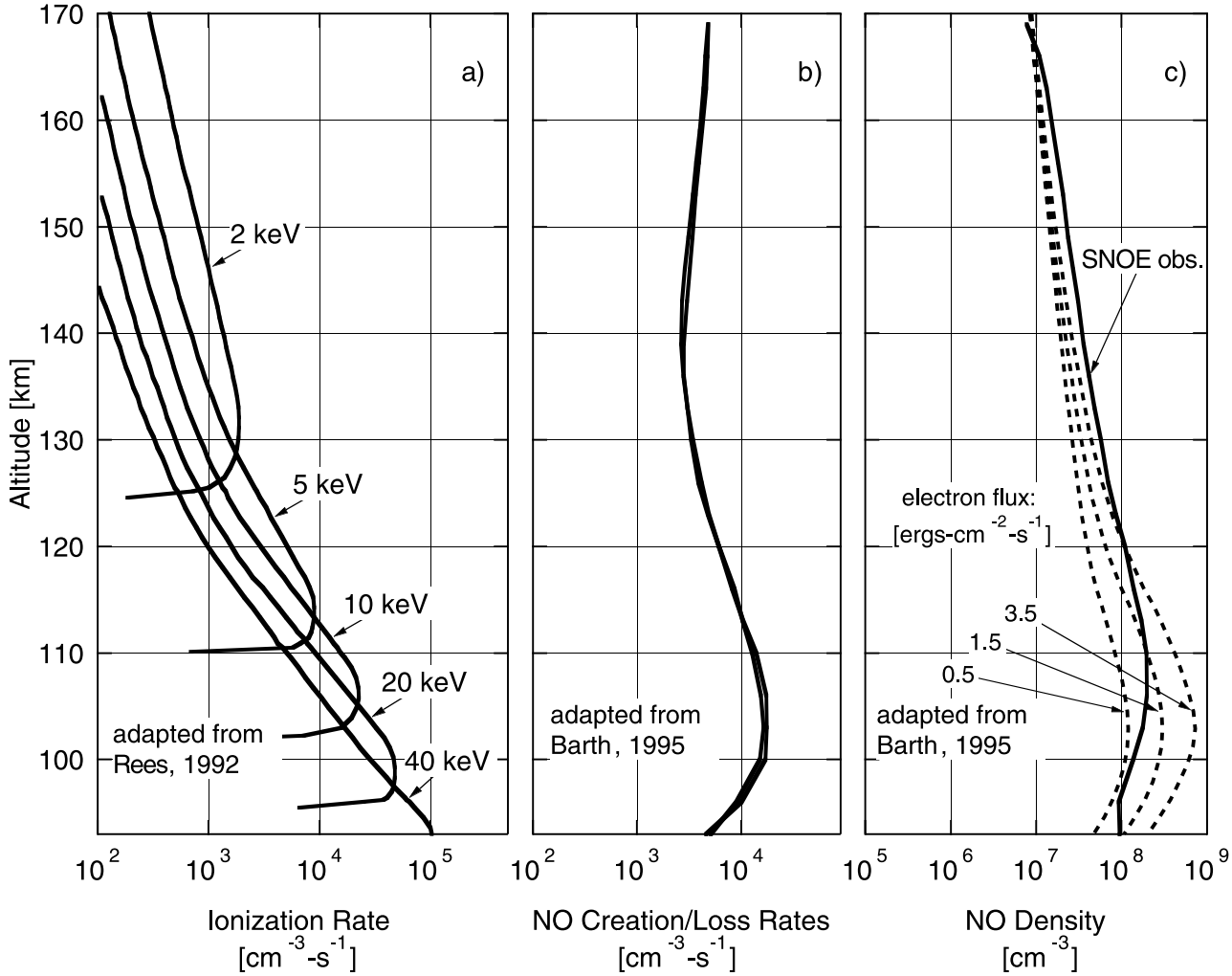

Figure 6. Altitude profiles for various parameters. (a) The modeled discrete auroral electron precipitation as a function of energy, for a unidirectional (along the magnetic field), monoenergetic electron flux of 10^8 el/cm^2-s (adapted from *Rees* [1992]). (b) Summed creation and loss rates of nitric oxide due to various physical and chemical processes, as described by *Barth* [1995]. (c) Modeled nitric oxide density for varying levels of incident electron flux [from *Barth*, 1995], along with the daily-averaged observed SNOE nitric oxide density (50°–85° magnetic latitude) over the first 3 years of the SNOE mission.

NO density at various altitudes finds the highest correlation between these data sets to occur at a significantly higher altitude (~126 km) than expected. At this altitude the correlation coefficient reaches 0.66, as shown in Figure 7. The variation in the correlation coefficient between the X-ray emissions and the NO density as a function of altitude is likely caused by variations in the NO production and loss rates. At higher altitudes (around 130 km and above), Joule heating can be an important source of nitric oxide production. Joule heating at these altitudes causes the reaction between ground state nitrogen and molecular oxygen to be faster than the reaction between excited state atomic nitrogen with molecular oxygen (the dominant source between 100 and 123 km) [*Siskind et al.*, 1989a, 1989b], leading to a greater efficiency of NO production due to magnetospheric interactions. In the upper atmosphere, Joule heating (predominantly due to Pedersen currents) and X-ray emissions (due to energetic electron precipitation, as part of the same current system) are expected to be positively correlated, although direct evidence is rather weak. Joule heating is proportional to the average of the square of the horizontal electric field. Continuous observations of the electric field and conductivities over the entire polar region have not yet been achieved. Theoretical and computational studies [*Siskind et al.*, 1989a, 1989b; *Codrescu et al.*, 1995, and references therein] have provided a solid foundation, but many details still need to be included. Rocket experiments [e.g., *Evans et al.*, 1977; *Theile et al.*, 1981] and incoherent scatter radar measurements [e.g., *Thayer*, 1998] have also helped to determine Joule heating rates during specific times and in specific locations. However, both of these methods are of limited temporal and spatial coverage. As a result, Joule heating rates can be difficult to ascertain. Instead, the geomagnetic auroral electrojet (*AE*) indices are often used as a proxy for the Joule heating rate [*Perreault and Akasofu*, 1978; *Akasofu*, 1981; *Ahn et al.*, 1983, 1989; *Baumjohann*

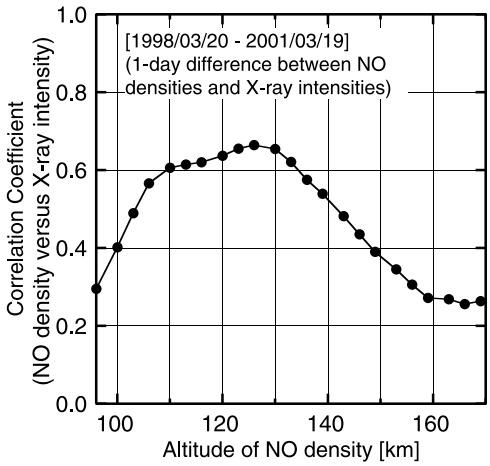

Figure 7. Correlation coefficient between the daily-averaged nitric oxide (delayed by 1 day) and the daily-averaged auroral bremsstrahlung (over the 3-year time span), as a function of the altitude of the nitric oxide.

and Kamide, 1984; *Richmond et al.*, 1990; *Cooper et al.*, 1995; *Lu et al.*, 1995, 1998]. The recent studies of *Østgaard et al.* [2002a, 2002b] have found good agreement between the Joule heating rates (determined from the *AE* index) and the electron precipitation determined using the Polar PIXIE and UltraViolet instrument observations for several substorm events.

[14] There has been observed a hemispheric asymmetry in the NO density as a function of season, such that the polar region with fewer hours of sunlight also tends to have a larger NO density [*Baker et al.*, 2001]. Since photodissociation is a major loss mechanism of NO, it is thought that this is the major cause of the hemispheric difference. On the basis of the Northern and Southern Hemisphere NO density ratios at 106 km altitude shown in Figure 5 of Baker et al., we are able to normalize the NO density values to account for the seasonal effect, using a sinusoidal function. Although no specific normalizing formula was provided, it has been determined that the sinusoidal function $NO' = NO \times (0.27 \times \cos((\text{day-}156)/365.25 \times 360) + 1)$ results in the highest correlation with the X-ray observations. This normalization slightly increases the correlation coefficient of Figure 5 from 0.57 to 0.63. It is somewhat expected that these correlations would not increase considerably, since the X-ray emissions also exhibit a seasonal effect [*Petrinec et al.*, 2000] similar to that observed by *Newell et al.* [1996, 1998], *Liou et al.* [1997], and *Collin et al.* [1998], which is thought to be due to differences in polar ionospheric conductivities (again caused by exposure to sunlight).

4. Summary

[15] The interaction of the magnetosphere and lower thermosphere in the north polar region has been examined using a broad statistical analysis comparing disparate data sets. In contrast to measuring auroral precipitation into the atmosphere with the limited duty cycle coverage for electron detectors on a low-altitude satellite, continuous worldwide coverage for periods of several hours duration was achieved with the PIXIE X-ray spectrometer on the POLAR satellite. From the calculated correlation coefficients using PIXIE and SNOE data, it has been shown that 20–40% of the variation of NO at northern high latitudes is due to variations in the auroral precipitation of energetic electrons. This is consistent with the recent statistical study by *Baker et al.* [2001], based upon SNOE observations and energetic (>25 keV) electron fluxes measured with the large-area microchannel plate sensor system (LICA) on board the Solar, Anomalous, and Magnetospheric Particle Explorer (SAMPEX) spacecraft. The correlation is raised by consideration of the delay times between data sets, as well as the altitude of the nitric oxide observations and seasonal variations, but illustrates the difficulty of comparing two data sets for which the timescales (e.g., the creation and losses of NO) change markedly with circumstances (orbital coverage, resolution of observations, etc.) and with altitude. Nevertheless, broad-based statistical studies such as this help us to more fully understand the coupling between the magnetosphere and upper atmospheric chemistry.

[16] **Acknowledgments.** The PIXIE work was supported by contract NASA NAS5-30372. The SNOE work was supported by cooperative agreement NCCW-0048 between NASA and the Universities Space Research Association and cooperative agreement 1500-01 between USRA and the University of Colorado. The authors gratefully acknowledge the World Data Center for providing the geomagnetic activity indices.

[17] Arthur Richmond thanks the reviewers for their assistance in evaluating this paper.

References

Ahn, B.-H., S.-I. Akasofu, and Y. Kamide, The Joule heat production rate and the particle energy injection rate as a function of the geomagnetic indices *AE* and *AL*, *J. Geophys. Res.*, *88*, 6275–6287, 1983.

Ahn, B.-H., H. W. Kroehl, Y. Kamide, and D. J. Gorney, Estimation of ionospheric electrodynamic parameters using ionospheric conductance deduced from bremsstrahlung X-ray image data, *J. Geophys. Res.*, *94*, 2565–2586, 1989.

Akasofu, S.-I., Energy coupling between the solar wind and the magnetosphere, *Space Sci. Rev.*, *28*, 121–190, 1981.

Anderson, P. C., D. L. McKenzie, D. W. Datlowe, J. D. Hawley, S. M. Petrinec, and M. Schulz, Polar cap X-rays and electrons under low density solar wind conditions: Coordinated PIXIE and DMSP observations on 11 May 1999, *Geophys. Res. Lett.*, *27*, 4021–4024, 2000.

Anderson, P. C., S. M. Petrinec, and K. Liou, Statistical patterns in X-ray and UV auroral emissions and energetic electron precipitation, *J. Geophys. Res.*, *106*, 5907–5911, 2001.

Bailey, S. M., C. A. Barth, M. J. Erickson, R. A. Kohnert, A. W. Merkel, E. M. Rodgers, S. C. Solomon, S. D. Straight, J. E. Vian, and T. N. Woods, Science instrumentation for the student nitric oxide explorer, *Proc. SPIE Int. Soc. Opt. Eng.*, *2830*, 264–273, 1996.

Baker, D. N., C. A. Barth, K. E. Mankoff, S. G. Kanekal, S. M. Bailey, G. M. Mason, and J. E. Mazur, Relationships between precipitating auroral zone electrons and lower thermospheric nitric oxide densities: 1998–2000, *J. Geophys. Res.*, *106*, 24,465–24,480, 2001.

Barth, C. A., Nitric oxide in the lower thermosphere, *Planet. Space Sci.*, *40*, 315–336, 1992.

Barth, C. A., Nitric oxide in the lower thermosphere, in *The Upper Mesosphere and Lower Thermosphere: A Review of Experiment and Theory*, *Geophys. Monogr. Ser.*, vol. 87, edited by R. M. Johnson and T. L. Killeen, pp. 225–233, AGU, Washington, D. C., 1995.

Baumjohann, W., and Y. Kamide, Hemispherical Joule heating and the *AE* indices, *J. Geophys. Res.*, *89*, 383–388, 1984.

Berger, M. J., and S. M. Seltzer, Bremsstrahlung in the atmosphere, *J. Atmos. Sol. Terr. Phys.*, *34*, 85–108, 1972.

Callis, L. B., Stratospheric studies consider crucial question of particle precipitation, *Eos Trans. AGU*, *82*, 297–301, 2001.

Callis, L. B., D. N. Baker, M. Natarajan, J. B. Blake, R. A. Mewaldt, R. S. Selesnick, and J. R. Cummings, A two-dimensional model simulation of downward transport of NO_y into the stratosphere: Effects on the 1994 austral spring O_3 and NO_y, *Geophys. Res. Lett.*, *23*, 1905–1908, 1996.

Codrescu, M. V., T. J. Fuller-Rowell, and J. C. Foster, On the importance of E-field variability for Joule heating in the high-latitude thermosphere, *Geophys. Res. Lett.*, *22*, 2393–2396, 1995.

Collin, H. L., W. K. Peterson, O. W. Lennartsson, and J. F. Drake, The seasonal variation of auroral ion beams, *Geophys. Res. Lett.*, *25*, 4071–4074, 1998.

Cooper, M. L., C. R. Clauer, B. A. Emery, A. D. Richmond, and J. D. Winningham, A storm time assimilative mapping of ionospheric electrodynamics analysis for the severe geomagnetic storm of November 8–9, 1991, *J. Geophys. Res.*, *100*, 19,329–19,342, 1995.

Crutzen, P. J., I. S. A. Isaksen, and G. C. Reid, Solar proton events: Stratospheric sources of nitric oxide, *Science*, *189*, 457–458, 1975.

Evans, D. S., N. C. Maynard, J. Trøim, T. Jacobsen, and A. Egeland, Auroral vector electric field and particle comparisons, 2, Electrodynamics of an arc, *J. Geophys. Res.*, *82*, 2235–2249, 1977.

Frahm, R. A., J. D. Winningham, J. R. Sharber, R. Link, G. Crowley, E. E. Gaines, D. L. Chenette, B. J. Anderson, and T. A. Potemra, The diffuse aurora: A significant source of ionization in the middle atmosphere, *J. Geophys. Res.*, *102*, 28,203–28,214, 1997.

Heath, D. F., A. J. Kreuger, and P. J. Crutzen, Solar proton events: Influence on stratospheric ozone, *Science*, *197*, 886–889, 1977.

Imhof, W. L., et al., The Polar Ionospheric X ray Imaging Experiment (PIXIE), *Space Sci. Rev.*, *71*, 385–408, 1995.

Imhof, W. L., M. Walt, R. R. Anderson, D. L. Chenette, J. D. Hawley, J. Mobilia, and S. M. Petrinec, The association of electron precipitation with auroral kilometric radiation, *J. Geophys. Res.*, *105*, 277–290, 2000.

Imhof, W. L., M. Walt, R. R. Anderson, J. D. Hawley, M. J. Brittnacher, S. M. Petrinec, and H. Matsumoto, Relationship between X-ray, ultraviolet, and kilometric radiation in the auroral region, *J. Geophys. Res.*, *106*, 10,479–10,492, 2001.

Jackman, C. H., A. R. Douglass, R. B. Rood, R. D. McPeters, and P. E. Meade, Effect of solar proton events on the middle atmosphere during the past two solar cycles as computed using a two-dimensional model, *J. Geophys. Res.*, *95*, 7417–7428, 1990.

Jackman, C. H., R. D. McPeters, G. J. Labow, E. L. Fleming, C. J. Praderas, and J. M. Russell, Northern Hemisphere atmospheric effects due to the July 000 solar proton event, *Geophys. Res. Lett.*, *28*, 2883–2886, 2001.

Lastovicka, J., Effects of geomagnetic storms in the lower ionosphere, middle atmosphere and troposphere, *J. Atmos. Sol. Terr. Phys.*, *58*, 831–843, 1996.

Liou, K., P. T. Newell, C.-I. Meng, M. Brittnacher, and G. K. Parks, Synoptic auroral distribution: A survey using Polar ultraviolet imagery, *J. Geophys. Res.*, *102*, 27,197–27,205, 1997.

Lorence, L. J., Jr., CEPXS/ONELD version 2.0: A discrete ordinates code package for general one-dimensional coupled electron-photon transport, *IEEE Trans. Nucl. Sci.*, *39*, 1031–1034, 1992.

Lorence, L. J., Jr., J. E. Morel, and G. D. Valdez, Results guide to CEPXS/ONELD: A one-dimensional coupled electron-photon discrete ordinates code package version 1.0, *Rep. SAND89-2211*, Sandia Natl. Lab., Albuquerque, N. M., 1990.

Lu, G., A. D. Richmond, B. A. Emery, and R. G. Roble, Magnetosphere-ionosphere-thermosphere coupling: Effect of neutral winds on energy transfer and field-aligned current, *J. Geophys. Res.*, *100*, 19,643–19,659, 1995.

Lu, G., et al., Global energy deposition during the January 1997 magnetic cloud event, *J. Geophys. Res.*, *103*, 11,685–11,694, 1998.

McPeters, R. D., A nitric oxide increase observed following the July 1972 solar proton event, *Geophys. Res. Lett.*, *13*, 667–670, 1986.

Minschwaner, K., and D. E. Siskind, A new calculation of nitric oxide photolysis in the stratosphere, mesosphere, and lower thermosphere, *J. Geophys. Res.*, *98*, 20,401–20,412, 1993.

Murray, J. E., K. Yoshino, J. R. Esmond, W. H. Parkinson, Y. Sun, A. Dalgarno, A. P. Thorne, and G. Cox, Vacuum ultraviolet Fourier transform spectroscopy of the $\delta(0,0)$ and $\beta(7,0)$ bands of NO, *J. Chem. Phys.*, *101*, 62–73, 1994.

Newell, P. T., C.-I. Meng, and K. M. Lyons, Suppression of discrete aurorae by sunlight, *Nature*, *381*, 766–767, 1996.

Newell, P. T., C.-I. Meng, and S. Wing, Relation to solar activity of intense aurorae in sunlight and darkness, *Nature*, *393*, 342–344, 1998.

Østgaard, N., J. Stadsnes, J. Bjordal, R. R. Vondrak, S. A. Cummer, D. L. Chenette, G. K. Parks, M. J. Brittnacher, and D. L. McKenzie, Global scale electron precipitation features seen in UV and X rays during substorms, *J. Geophys. Res.*, *104*, 10,191–10,204, 1999.

Østgaard, N., J. Stadsnes, J. Bjordal, R. R. Vondrak, S. A. Cummer, D. L. Chenette, M. Schulz, and J. G. Pronko, Cause of the localized maximum of X-ray emission in the morning sector: A comparison with electron measurements, *J. Geophys. Res.*, *105*, 20,869–20,885, 2000a.

Østgaard, N., et al., Global X-ray emission during an isolated substorm—A case study, *J. Atmos. Sol. Terr. Phys.*, *62*, 889–900, 2000b.

Østgaard, N., G. Germany, J. Stadsnes, and R. R. Vondrak, Energy analysis of substorms based on remote sensing techniques, solar wind measurements, and geomagnetic indices, *J. Geophys. Res.*, *107*(A9), 1233, 10.1029/2001JA002002, 2002a.

Østgaard, N., R. R. Vondrak, J. W. Gjerloev, and G. Germany, A relation between the energy deposition by electron precipitation and geomagnetic indices during substorms, *J. Geophys. Res.*, *107*(A9), 1246, 10.1029/2001JA002003, 2002b.

Perreault, P., and S.-I. Akasofu, A study of geomagnetic storms, *Geophys. J. R. Astron. Soc.*, *54*, 547–573, 1978.

Petrinec, S. M., D. L. Chenette, J. Mobilia, M. A. Rinaldi, and W. L. Imhof, Statistical X ray auroral emissions—PIXIE observations, *Geophys. Res. Lett.*, *26*, 1565–1568, 1999.

Petrinec, S. M., W. L. Imhof, D. L. Chenette, J. Mobilia, and T. J. Rosenberg, Dayside/nightside auroral X ray emission differences: Implications for ionospheric conductance, *Geophys. Res. Lett.*, *27*, 3277–3279, 2000.

Randall, C. E., D. W. Rusch, R. M. Bevilacqua, K. W. Hoppel, and J. D. Lumpe, Polar Ozone and Aerosol Measurement (POAM) II stratospheric NO_2, 1993–1996, *J. Geophys. Res.*, *103*, 28,361–28,371, 1998.

Randall, C. E., D. E. Siskind, and R. M. Bevilacqua, Stratospheric NO_x enhancements in the Southern Hemisphere vortex in winter/spring of 2000, *Geophys. Res. Lett.*, *28*, 2385–2388, 2001.

Reagan, J. B., R. E. Meyerott, R. W. Nightingale, R. C. Gunton, R. G. Johnson, J. E. Evans, W. L. Imhof, D. F. Heath, and A. J. Kreuger, Effects of the August 1972 solar particle events on stratospheric ozone, *J. Geophys. Res.*, *86*, 1473–1494, 1981.

Rees, M. H., Auroral energy deposition rate, *Planet. Space Sci.*, *40*, 299–313, 1992.

Reid, G. C., S. Solomon, and R. R. Garcia, Response of the middle atmosphere to the solar proton events of August–December, 1989, *Geophys. Res. Lett.*, *18*, 1019–1022, 1991.

Richmond, A. D., et al., Global measures of ionospheric electrodynamic activity inferred from combined incoherent scatter radar and ground magnetometer observations, *J. Geophys. Res.*, *95*, 1061–1071, 1990.

Siskind, D. E., C. A. Barth, and R. G. Roble, The response of thermospheric nitric oxide to an auroral storm, 1, Low and middle latitudes, *J. Geophys. Res.*, *94*, 16,885–16,898, 1989a.

Siskind, D. E., C. A. Barth, D. S. Evans, and R. G. Roble, The response of thermospheric nitric oxide to an auroral storm, 2, Auroral latitudes, *J. Geophys. Res.*, *94*, 16,899–16,911, 1989b.

Solomon, S., G. C. Reid, D. W. Rusch, and R. J. Thomas, Mesospheric ozone depletion during the solar proton event of July 13, 1982, 2, Comparison between theory and measurements, *Geophys. Res. Lett.*, *10*, 257–260, 1983.

Solomon, S. C., et al., The student nitric oxide explorer, *Proc. SPIE Int. Soc. Opt. Eng.*, *2810*, 121–132, 1996.

Solomon, S. C., C. A. Barth, and S. M. Bailey, Auroral production of nitric oxide measured by the SNOE satellite, *Geophys. Res. Lett.*, *26*, 1259–1262, 1999.

Thayer, J. P., Height-resolved Joule heating rates in the high-latitude *E* region and the influence of neutral winds, *J. Geophys. Res.*, *103*, 471–487, 1998.

Theile, B., R. Boström, A. Dumbs, K. U. Grossman, D. Krankowsky, P. Lämmerzahl, G. Marklund, E. Neske, G. Schmidtke, and K. Wilhelm, In situ measurements of heating parameters in the auroral ionosphere, *Planet. Space Sci.*, *29*, 455–468, 1981.

Vitt, F. M., and C. H. Jackman, A comparison of sources of odd nitrogen production from 1974 through 1993 in the Earth's middle atmosphere as calculated using a two-dimensional model, *J. Geophys. Res.*, *101*, 6729–6739, 1996.

Weeks, L. H., R. S. CuiKay, and J. R. Corbin, Ozone measurements in the mesosphere during the solar proton event of November 2, 1969, *J. Atmos. Sci.*, *29*, 1138–1142, 1972.

D. N. Baker, C. A. Barth, and K. D. Mankoff, Laboratory for Atmospheric and Space Physics, Boulder, CO 80303-7814, USA.

W. L. Imhof and S. M. Petrinec, Lockheed Martin Advanced Technology Center, Palo Alto, CA 94304-1181, USA. (petrinec@spasci.com)

J. G. Luhmann, Space Sciences Laboratory, University of California, Berkeley, Berkeley, CA 94720, USA.